

Supplementary Information

Colour and SERS Patterning Using Core–Satellite Nanoassemblies

Sungwoon Lee, Minkyu Kim, and Sangwoon Yoon*

Department of Chemistry, Chung-Ang University, 84 Heukseok-ro, Dongjak-gu, Seoul 06974, Korea

*E-mail: sangwoon@cau.ac.kr

1. Experimental Methods

1.1 Materials

The following materials were purchased and used as received: Gold(III) chloride trihydrate ($\geq 99.9\%$, Sigma Aldrich), sodium citrate tribasic dehydrate ($\geq 99.0\%$, Sigma Aldrich), (3-aminopropyl)trimethoxysilane (APTMS, 97%, Sigma Aldrich), 1,8-octanedithiol (C8DT, $\geq 97\%$, Sigma Aldrich), 4-aminobenzenethiol (ABT, 97%, Sigma Aldrich), 4-mercaptobenzoic acid (MBA, 99%, Sigma Aldrich), sodium hydroxide ($\geq 98\%$, Sigma Aldrich), RBS detergent solution (35 concentrate, Sigma Aldrich), ethanol ($\geq 99.9\%$, Duksan Chemical), methanol ($\geq 99.8\%$, Sigma Aldrich), hydrochloric acid (EP grade, Duksan Chemical), and water (HPLC grade, J. T. Baker).

1.2 Synthesis of AuNPs

Citrate-capped gold nanoparticles (AuNPs, 17-nm diameter) were prepared using the Turkevich method.¹ More specifically, a solution of sodium citrate (34 mM, 50 mL) was added to a solution of HAuCl_4 (0.27 mM, 950 mL) and allowed to react for 30 min at 100 °C with vigorous stirring. Upon formation of the nanoparticles, the solution colour changed from yellow to wine red. These nanoparticles served as satellite nanoparticles for the assembly process.

Table S1. Nanoparticle growth conditions

Step	Added reagent	Added volume (mL)	Reaction time (min)
Seed	Citrate	6	
	HAuCl_4	1	
	H_2O	150	
1 st growth	HAuCl_4	1	30
	HAuCl_4	1	30
2 nd growth	Citrate	4	5
	HAuCl_4	2	30
	HAuCl_4	2	30
	H_2O	150	
3 rd growth	Citrate	6	5
	HAuCl_4	3	30
	HAuCl_4	3	30
	H_2O	300	
4 th growth	Citrate	10	5
	HAuCl_4	5	30
	HAuCl_4	5	30
	H_2O	356	

For synthesis of large AuNPs (*i.e.* core AuNPs in the assembly), we employed the seeded growth method developed by Puntès and co-workers.² Firstly, nanoparticle seeds were prepared by the rapid

addition of solutions of sodium citrate (60 mM, 6 mL) and HAuCl₄ (25 mM, 1 mL) to boiling water (150 mL). The seed particles were then grown into AuNPs with a diameter of 66 nm by the sequential addition of the various reagents listed in Table S1.

1.3 Characterization of AuNPs

The sizes of the AuNPs were measured using transmission electron microscopy (TEM). The produced core and satellite AuNPs were found to have diameters of 65.5 ± 7.9 nm (1002-particle average) and 16.8 ± 1.2 nm (177-particle average), respectively (Figure S1).

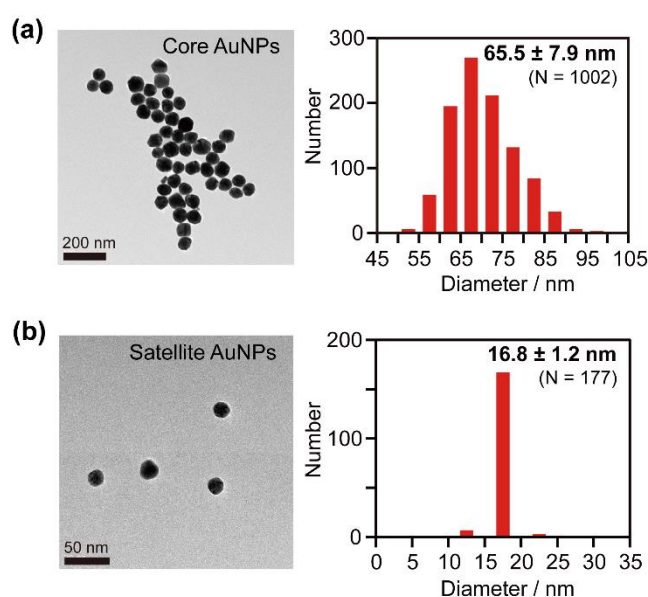


Figure S1. Representative TEM images and size distributions of (a) core AuNPs, and (b) satellite AuNPs.

1.4 Spatially Controlled Assembly of AuNPs into Core–Satellite Structures

For assembly of the nanoparticles, we employed a previously reported method with modifications.³

Step 1: Glass slides (HSU-1000412, thickness of 1 mm, Marienfeld, Germany) were cut into specimens measuring 12.5 mm × 25 mm and then cleaned by immersion in RBS solution at 90 °C. After rinsing, the glasses were immersed in a solution of APTMS (1% v/v, 5 mL) for 0.5 h to achieve amine-functionalisation of their surfaces.

Step 2: Immersion of the glass slides in an aqueous solution of the core AuNPs (66 nm, 35 pM, 5 mL) for 5 h led to adsorption of the citrate-capped AuNPs onto the amine-coated glass slides *via* electrostatic interactions.

Step 3: Following adsorption of the core AuNPs onto the glass slides, the free (unbound) amine functional groups present on the glass slides were removed using NaOH. For this ‘masked desilanisation’ process, the AuNP-adsorbed glass slides were immersed in a solution of NaOH (10 mM, 5 mL) for 5 h. Peeling of the amine coating during this process (with the exception of the area where the core AuNPs resided) prevented the satellite AuNPs from adsorbing onto the glass slide in a later step.

Step 4: The core AuNPs remaining on the glass slides were then surface-functionalised with thiol or amine groups using either C8DT or ABT, respectively. More specifically, the AuNP/glass was immersed in an ethanolic solution of C8DT or ABT (1 mM, 5 mL) for 1 h.

Step 5: UV irradiation was then employed to induce photooxidative desorption of the thiols from the core AuNPs and remove the linkers to the satellite AuNPs at the desired spots.⁴ For this step, the thiol-AuNP/glass was placed in ethanol (50 mL) in a petri dish and subjected to UV irradiation either directly or through optical masks. UV light ($\lambda \leq 365$ nm) was delivered to the desired spot by use of a light guide from a Hg–Xe lamp (L9566-01A, LC8, Hamamatsu). The thiol-AuNP/glass was illuminated from the top by positioning the output port of the light guide typically 1.5 cm above the sample surface. The power at the sample corresponded to 650 mW/cm². We found the optimal irradiation time to be 1 h for such direct illumination conditions. Figure S2 shows that the best colour pattern is obtained when the thiol-functionalised core AuNPs are irradiated for 1 h in Step 5. Exposure to UV for less than 1 h leaves the thiol linkers on the core AuNPs, leading to the partial formation of core–satellite nanoassemblies in the irradiated region, which makes the colour less clearly distinguishable between the irradiated and the unirradiated areas. In contrast, overexposure (90 min) makes the boundary blurry.

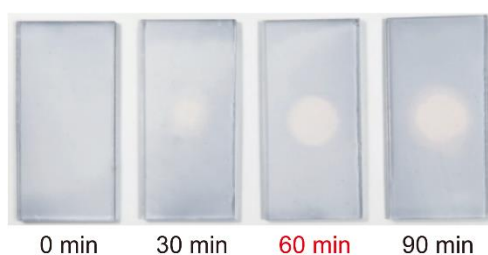


Figure S2. Colour patterns obtained by following the procedure presented in Figure 1, with the irradiation time in Step 5 changing from 0 to 90 min. Irradiation for 1 h yields the best colour contrast between the core AuNP monomers in the irradiated area and the core–satellite nanoassemblies in the unirradiated area.

For illuminating a wider area over centimetre-scale optical masks, we moved the position of the light guide to 4.8 cm above the sample surface. Consequently, the power dropped to 190 mW/cm² at the sample and thus, we extended the irradiation time to 4.5 h. The masks were composed of screen-printed carbon coatings on thin glasses (Exax, Korea, Figure S3). For micrometre-scale patterning, we used TEM grids (G400-C3, Gilder) as masks.

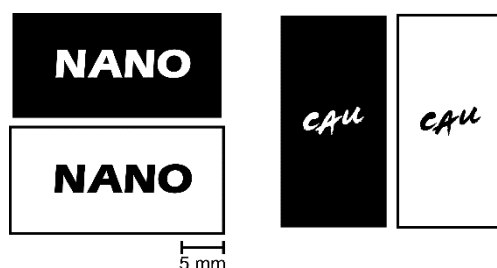


Figure S3. Optical masks used for colour patterning with core–satellite nanoassemblies in Figure 3a.

Step 6. The irradiated AuNP/glass samples were then transferred to a solution containing the satellite AuNPs (17 nm) and allowed to stand in this solution (4.1 nM, 5 mL) for 3 h. The core–satellite nanoassemblies were formed only in the unirradiated region where the C8DT or ABT linkers on the core AuNPs remained intact. As linkers were removed from some areas by UV irradiation in a previous step, the core AuNPs remained as monomers in the irradiated regions, yielding core–satellite nanoassemblies and core AuNPs distributed along the irradiation pattern.

1.5 Measurements

The resulting nanoparticle distribution and colour contrast were measured *via* digital photography (QX-100, Sony), scanning electron microscopy (S-4800, Hitachi or Sigma, Carl Zeiss), UV-vis spectroscopy (Lambda 25, PerkinElmer), and dark-field microscopy (BX 51, Olympus, equipped with an MPLAN BD 100× NA 0.90 objective and a CMOS camera, Chameleon 3, FLIR). The Raman spectra of the monomers in the irradiated areas and the core–satellite nanoassemblies in the unirradiated areas were acquired *via* Raman microscopy (Alpha300-SR, Witec) at an excitation wavelength of 633 nm and with a total exposure time of 2 s. For Raman mapping, 60 × 60 spots were selected over a 120 μm × 120 μm area. A set of spectra was obtained, and the intensity was mapped with respect to the peak at 1078 cm⁻¹.

2. SERS from Patterned Core–Satellite Nanoassemblies

2.1 SERS Spectra of ABT (or DMAB)

The SERS spectra acquired from the bar region of the sample in Figure 4a are in fact from 4,4'-dimercaptoazobenzene (DMAB), rather than ABT. As reported previously,⁵ ABT readily transforms to DMAB by plasmon excitation. The DMAB Raman spectrum features three characteristic peaks at 1140, 1388, and 1438 cm^{-1} , that were previously assigned to the charge transfer b2-mode peaks,⁶ but turned out to be the peaks of the plasmon-driven reaction product, DMAB.⁵ We observe all three peaks in our SERS spectrum from the core–satellite nanoassemblies in Figure 4a, also indicated by the red asterisks in Figure S4. However, we simply refer to the spectrum of DMAB as the spectrum of ABT in the main manuscript because DMAB is formed from ABT and either spectrum serves equally well to find the spatial distribution of the core–satellite nanoassemblies on the glass slide.

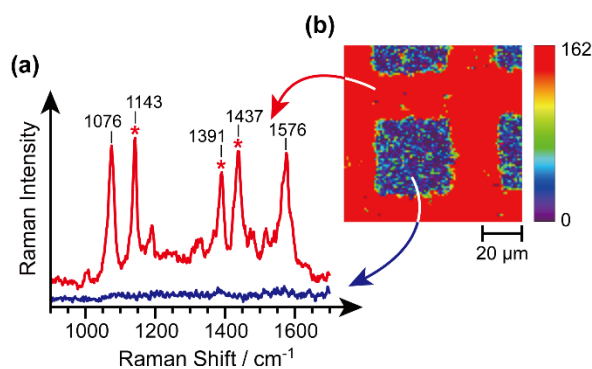


Figure S4. The peak positions of the SERS spectra acquired from the bar region of the patterned sample, presented in Figure 4a. The red asterisks indicate the characteristic Raman peaks of DMAB that is produced from ABT by plasmon excitation.

2.2 SERS Enhancement Factor (EF) for the Core–Satellite Nanoassemblies

Although it is not directly related to the main theme of this paper, we can estimate the SERS enhancement factor (EF) for the core–satellite nanoassembly structures prepared on the glass slide. The SERS EF refers to the ratio between the Raman signal intensity of a molecule in the presence of nanoparticles and that of the molecule in the absence of nanoparticles:

$$EF_{\text{expt}} = \frac{I_{\text{SERS}}/N_{\text{SERS}}}{I_{\text{NR}}/N_{\text{NR}}},$$

where I_{SERS} and I_{NR} are the SERS intensity and normal (unenhanced) Raman intensity, respectively; N_{SERS} and N_{NR} are the number of molecules being probed in SERS and normal Raman without nanoparticles, respectively.

We obtained Raman spectra of ABT in a capillary tube using the same laser and the same Raman acquisition conditions (Figure S5). From the focal conditions (beam waist 3 μm , confocal parameter 83 μm),⁷ we estimate that the probe volume corresponds to 2206 μm^3 and, hence, the N_{NR} for 2 M ABT is 2.7×10^{12} . For N_{SERS} , the molecules in the nanogaps between the core and the satellite molecules cause SERS. From the gap area [$227 \text{ nm}^2 = \pi \times (17/2 \text{ nm})^2$], the number of gaps in the probe region ($1680 = 12 \text{ satellites per core} \times 140 \text{ assemblies in the } 6\text{-}\mu\text{m focal area}$), and the occupation area of an ABT molecule (0.2 nm^2), we calculate the N_{SERS} , 1.9×10^6 . Therefore, the experimental EF is estimated at 3×10^7 .

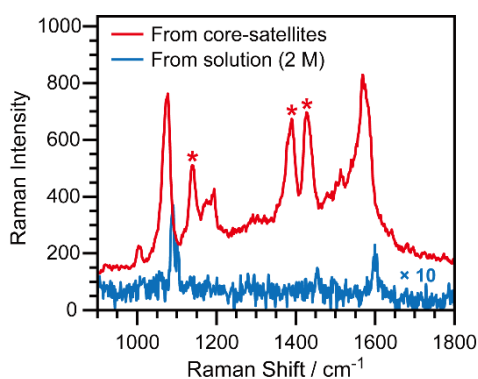


Figure S5. Raman spectra acquired from (a) core–satellite nanoassemblies with ABT linkers, prepared on the glass slide as in Figure 4, and (b) 2 M ABT solution in ethanol in a capillary tube. Background spectra (glass and ethanol) were subtracted from each spectrum to display the spectral features of ABT only. The red asterisks indicate the characteristic Raman peaks of DMAB which is readily produced from ABT by plasmon excitation of nanostructures (see Section 2.1). The SERS EF is measured for the CS stretching mode near 1076 cm^{-1} .

2.3 FDTD Simulation and Theoretical SERS EF

We performed the finite-difference time domain (FDTD) simulation to calculate the local field distribution and enhancement, induced by plasmon excitation of core–satellite nanoassemblies. We constructed a core–satellite nanoassembly that consists of a 66-nm core AuNP at the center and 12 satellite AuNPs (17 nm) around the core AuNP with a gap distance of 1.0 nm (Figure S6a). This structure resembles the experimentally prepared core–satellite AuNPs with the ABT as a linker. Light with a wavelength of 633 nm propagates from the top with a polarization shown as E_0 in Figure S6. The dielectric function of Au was modeled from the Johnson and Christy values. The total simulation

region was set to $1500 \text{ nm} \times 1500 \text{ nm} \times 1500 \text{ nm}$, and the override region ($130 \text{ nm} \times 130 \text{ nm} \times 130 \text{ nm}$) with a mesh size of 0.25 nm was set enclosing the assembly to improve the accuracy for the calculation of local electric fields inside the nanogaps.

Figure S6 shows the plasmon-induced electric field distribution for a core–satellite nanoassembly and a core AuNP monomer. Local field enhancement is the largest at the nanogaps between the core and the satellite AuNPs, particularly when the AuNPs are aligned with the polarization of incident light. The theoretical SERS EF (EF_{calc}) is proportional to the fourth power of the local electric fields (E_{loc}) that form in the nanogaps or around the nanoparticles because both the incident and the scattering fields are enhanced:⁸

$$EF_{calc} = \left| \frac{E_{loc}}{E_0} \right|^4.$$

From the simulation, we obtain the theoretical SERS EF, 2.0×10^7 and 5.2×10^2 for the core–satellite nanoassembly and the monomer AuNP, respectively. The theoretical SERS EF is in excellent agreement with the experimental SERS EF (3×10^7) for the core–satellite nanoassemblies. Furthermore, the stark difference in SERS EF between the core–satellite nanoassemblies and the AuNP monomers provides a basis for SERS patterning using the method developed in this study.

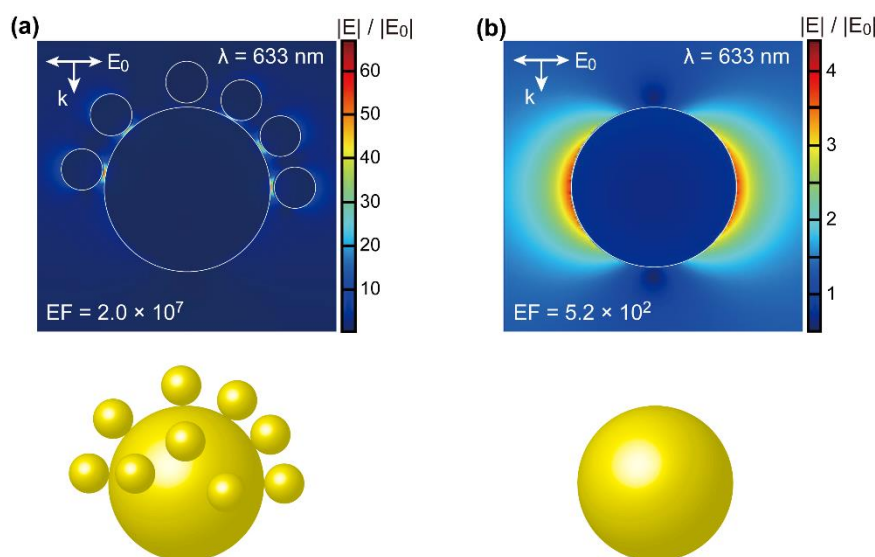


Figure S6. Simulated electric field distribution for (a) a core–satellite nanoassembly, and (b) a core AuNP monomer, induced by plasmon excitation at 633 nm . k and E_0 represent the propagation and polarization vector of incident light, respectively. The calculated SERS EF values, $(|E_{max}/E_0|^4)$, for each nanostructure are included in the figure.

3. Application of the Patterned Nanoassembly Substrates as SERS Sensors

Our method presented in this paper allows one to prepare SERS-active core–satellite nanoassemblies at specific places. The resulting patterned substrates (*e.g.*, in lateral flow microchip) can be applied as SERS sensors. As a proof of concept, here we demonstrate the potential applicability of our method to SERS sensing.

We prepared a glass substrate where core AuNP monomers were located in the center (irradiated region) while the core–satellite nanoassemblies were distributed in the unirradiated region (Figure S7a). To minimize the interference in the Raman signal by the linkers, we used a less Raman-active molecule as a linker, namely C8DT, for the core–satellite nanoassemblies. Indeed, we did not observe Raman signal from either the monomer or the core–satellite region (Figure S7a). Then, we immersed the substrate in an analyte solution (in this case, 4-mercaptobenzoic acid (MBA), 1 mM) for 1 h. After washing, we acquired Raman spectra again from the substrate. We observed the SERS spectra of MBA from the core–satellite region while no detectable signal was observed from the monomer region (Figure S7b). Raman signal was detected when we lowered the concentration of the MBA solution to 0.1 mM and 0.01 mM. This demonstration clearly indicates that the patterned core–satellite nanoassembly substrates can be used as position-specific SERS sensors for detecting analytes.

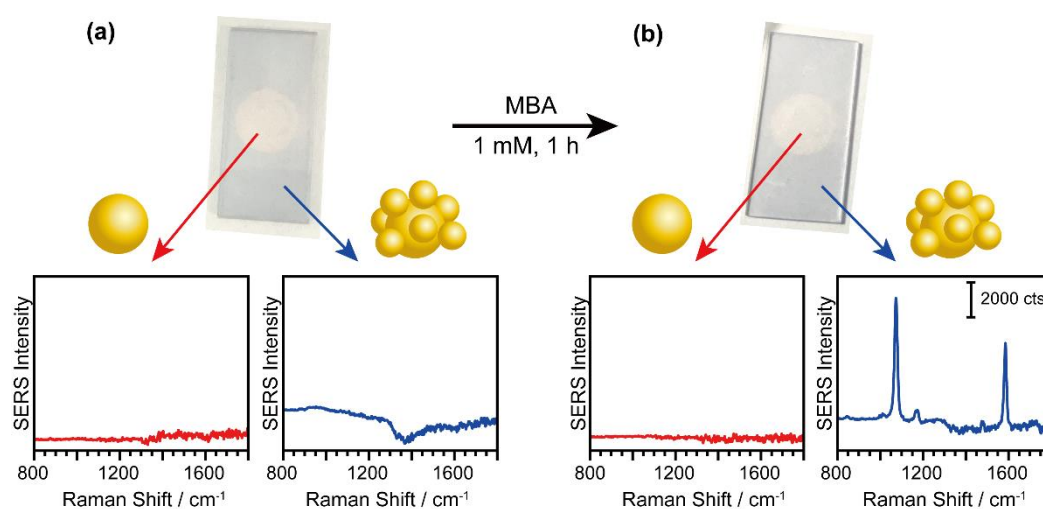


Figure S7. The proof-of-concept experiment on SERS sensing of analytes using the patterned core–satellite nanoassembly substrate. (a) A SERS substrate prepared using the method outlined in Figure 1. Core AuNP monomers are located at the center (red); core–satellite nanoassemblies are formed in the other area (dark blue). C8DT molecules were used as the linker for the core–satellite nanoassemblies. No Raman signal was detected from either the monomer or the core–satellite region. (b) The SERS substrate after immersion in 4-mercaptobenzoic acid (MBA, 1 mM, 1h). The SERS signal of MBA is detected from the core–satellite nanoassembly region whereas

no Raman signal is observed from the monomer AuNP region, demonstrating the position-specific detection of analytes.

References

1. J. Turkevich, P. C. Stevenson and J. Hillier, *Discuss. Faraday Soc.*, 1951, **11**, 55.
2. N. G. Bastús, J. Comenge and V. Puntes, *Langmuir*, 2011, **27**, 11098.
3. H. Cha, J. H. Yoon and S. Yoon, *ACS Nano*, 2014, **8**, 8554.
4. H. Jung, H. Cha, D. Lee and S. Yoon, *ACS Nano*, 2015, **9**, 12292.
5. Y.-F. Huang, H.-P. Zhu, G.-K. Liu, D.-Y. Wu, B. Ren and Z.-Q. Tian, *J. Am. Chem. Soc.*, 2010, **132**, 9244.
6. M. Osawa, N. Matsuda, K. Yoshii and I. Uchida, *J. Phys. Chem.*, 1994, **98**, 12702.
7. A. E. Siegman, *Lasers*, University Science Books, Palo Alto, California, U.S.A., 1986.
8. E. C. Le Ru and P. G. Etchegoin, *Principles of Surface-Enhanced Raman Spectroscopy and Related Plasmonic Effects*, Elsevier, Oxford, U.K., 2009.